Available online at www.sciencedirect.com

SciVerse ScienceDirect

Proceedings of the Combustion Institute 34 (2013) 1241–1249

Proceedings of the Combustion Institute

www.elsevier.com/locate/proci

Large-eddy simulation/probability density function modeling of a non-premixed CO/H_2 temporally evolving jet flame

Yue Yang [a,b,*], Haifeng Wang [a], Stephen B. Pope [a], Jacqueline H. Chen [b]

[a] *Sibley School of Mechanical and Aerospace Engineering, Cornell University, Ithaca, NY 14853, USA*
[b] *Combustion Research Facility, Sandia National Laboratories, Livermore, CA 96551-0969, USA*

Available online 28 September 2012

Abstract

We report a large-eddy simulation (LES)/probability density function (PDF) study of a non-premixed CO/H_2 temporally-evolving turbulent planar jet flame, which has previously been studied using direct numerical simulations (DNS) with a skeletal chemical mechanism. The flame exhibits strong turbulence–chemistry interactions resulting in local extinction followed by re-ignition. In this study, the filtered velocity field in LES and the PDF transport equations with the interaction-by-exchange with the mean (IEM) mixing model (with molecular transport) are solved by the highly-scalable NGA/HPDF codes with second-order accuracy in space and time. The performance of the hybrid LES/PDF methodology is assessed through detailed *a posteriori* comparisons with DNS of the same flame. The comparison shows overall good agreement of the temporal evolution of the temperature and mass fractions of major chemical species, as well as the prediction of local extinction and re-ignition. The modeling of multi-scalar mixing is analyzed using the DNS and LES/PDF results. The DNS results exhibit an attracting manifold of the streamlines of the diffusion velocity in composition space, and the LES/PDF results show qualitative agreement on the manifold and joint PDFs of compositions.

Keywords: Large-eddy simulation; Probability density function methods; Turbulent non-premixed jet flame; Multi-scalar mixing

1. Introduction

The numerical simulation of turbulent reacting flows has emerged as a powerful technique for investigating fundamental problems and developing predictive models in turbulent combustion. Among the simulation methods, direct numerical simulation (DNS) requires minimal modeling, but is restricted to simple geometries and a moderate range of scales. The computational cost of the DNS of a high-Reynolds-number turbulent reacting flow with detailed chemistry is still very expensive, e.g., such a DNS run may take millions of CPU hours on a supercomputer [1]. Compared to DNS, the hybrid large-eddy simulation (LES) and probability density function (PDF) method involves more extensive modeling, but its computational cost is much lower than DNS, so it is

* Corresponding author. Address: 138 Upson Hall, Cornell University, Ithaca, NY 14853, USA. Fax: +1 (607) 255 1222.
E-mail address: yy463@cornell.edu (Y. Yang).

1540-7489/$ - see front matter © 2012 The Combustion Institute. Published by Elsevier Inc. All rights reserved.
http://dx.doi.org/10.1016/j.proci.2012.08.015

applicable to practical devices such as gas turbine combustors and internal combustion engines [2–4]. In LES, large-scale motions are directly computed while small-scale or subgrid scale (SGS) motions are not explicitly represented, but their effects on the large scales are modeled. The turbulence–chemistry interactions are modeled by the PDF method [5–7]. In addition, the computation of combustion chemistry can be significantly accelerated by the *in situ* adaptive tabulation (ISAT) algorithm [8,9]. Besides the LES/PDF modeling approach, recent progress of LES of turbulent combustion is reviewed in [10].

In the modeling approaches of LES/PDF, the SGS modeling of turbulent reacting flows is very challenging owing to the wide range of length and time scales involved in turbulence and the strong non-linear nature of chemical reactions. The hybrid LES/PDF method provides a promising approach to simulate turbulent combustion with detailed chemistry [11–13]. In the PDF methodology, the chemical reaction is treated exactly but the mixing term is unclosed. The modeling of mixing is critical in non-premixed combustion, because molecular mixing of reactants is necessary to allow chemical reaction, and reaction rates of compositions have highly non-linear dependencies on their concentrations and on temperature. Additionally, the interaction of finite-rate chemistry with strong mixing can lead to local extinction, which may cause harmful emissions and flame instability, and is challenging for the SGS modeling.

The turbulent mixing of a passive scalar [14] and the evaluation of several existing mixing models [15–17] have been investigated in some canonical turbulent flows for Reynolds averaged Navier–Stokes simulation (RANS)/PDF and LES/PDF. In turbulent reacting flows, there are at least three scalars involved, i.e., two reactants and one product. However, most mixing models use only composition-space variables and do not take into account the spatial structure of the scalars. To address this issue, the inert mixing of two or three passive scalars is studied in experiments [18] and DNS [19,20], followed by the validation of several mixing models [21], but there are lack of *a priori* and *a posteriori* tests of the multi-scalar modeling in turbulent reacting flows. The existing DNS database of a gas-phase, non-premixed CO/H_2 temporally evolving jet flame at a low Damköhler number [22] stores the whole temporal–spatial information of compositions (about 64 Gbytes per step). This is usually not available in experiments and provides a valuable opportunity to investigate the modeling of multi-scalar mixing in LES/PDF. Additionally, this DNS is used to estimate the mixing time scale of compositions [22] and the approximation of scalar dissipation rates [23]. A variant of the one-dimensional turbulence model is applied to the DNS and the model can reproduce the spread rate of the jet flame and qualitatively predict the level of local extinction [24].

The goal of this study is to assess the capabilities of LES/PDF by making detailed comparisons with DNS of the same flame. The performance of the LES/PDF is assessed via *a posteriori* comparisons with DNS including the prediction of local extinction and re-ignition in a non-premixed CO/H_2 temporally evolving turbulent jet flame. The multi-scalar mixing in DNS and LES/PDF will be analyzed and discussed in detail.

2. Simulation overview

2.1. DNS

The DNS of a non-premixed CO/H_2 temporally evolving planar jet flame is preformed by Hawkes et al. [22]. The fuel is composed of 50% CO, 10% H_2 and 40% N_2 by volume, which represents syngas. The co-flow is composed of 25% O_2 and 75% N_2. The initial temperature of the co-flow is 500 K, and pressure is set to atmospheric. The multiple transport properties for 11 species and the skeletal CO/H_2 mechanism with 21 reaction steps based on a detail C1-kinetics are used [22].

A schematic of the DNS configurations is shown in Fig. 1. The computational domain is within a three-dimensional cuboid with size $L_x \times L_y \times L_z = 12H \times 14H \times 8H$, where H is the jet height. The boundary conditions are periodic in the streamwise direction x and the spanwise direction z, and outflow in the cross-stream direction y. The grid spacing Δx of the DNS is unform and equal in all the directions.

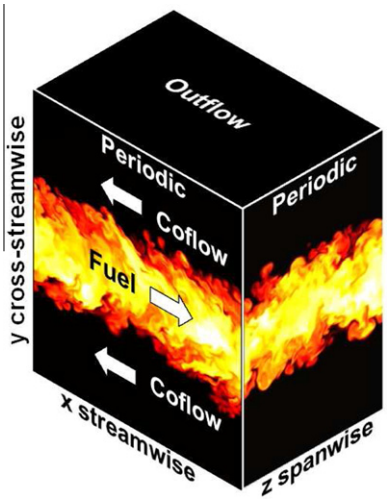

Fig. 1. Schematic of the DNS configurations [22] (with temperature contours at $t = 40t_j$ for $Re = 9079$).

The flow is statistically one-dimensional, with statistics varying only in the y-direction. Initially ($t = 0$) the flow consists of a slab of thickness H of fuel moving in the x-direction at the bulk velocity $U/2$ and on either side co-flows of the oxidizer moving in the opposite direction at $-U/2$. The characteristic time scale is defined as $t_j = H/U$. The evolution of the turbulent jet flame is triggered by small velocity fluctuations near the central jet. The statistics of the jet flame are independent of the initial condition after about $t = 20t_j$ [22]. Combustion is initialized by a laminar flamelet solution at an initial scalar dissipation rate $\chi = 0.75\chi_q$, where χ_q is the extinction scalar dissipation rate. The flow Reynolds number is defined by $Re = UH/\nu_f$ where ν_f is the kinematic viscosity of the pure fuel stream. Parameters of the runs in the present study are listed in Table 1. The Damköhler number is $Da = \chi_q t_j = 0.011$ for both Re cases, which is low enough to result in local extinction.

2.2. LES/PDF

The LES/PDF is a hybrid mesh–particle method. The NGA code [25] is used to solve the LES transport equations for mass and momentum on a uniform Cartesian grid with parameters listed in Table 1. The filtered velocity field $\tilde{\boldsymbol{u}}$ in LES is computed with second-order accuracy in space and time, where the tilde "∼" denotes density-weighted filtering with the LES filter width Δ that is equal to Δx of LES/PDF and eight times of Δx of DNS. The pressure Poisson equation is solved to enforce continuity. The dynamic SGS model is employed to obtain the turbulent SGS viscosity μ_T and diffusivity Γ_T [26]. The same boundary conditions of the DNS are applied, and the initial LES fields are filtered and interpolated from the DNS initial fields.

In reacting flows, the composition variable $\boldsymbol{\phi}$ contains n_s species mass fractions $Y = \{Y_\alpha, \alpha = 1,\ldots,n_s\}$ and enthalpy h. Using the new framework of the self-conditioned PDF [27], we define $f(\boldsymbol{\psi};\boldsymbol{x},t)$ to be the (one-point, one-time) density-weighted joint PDF of composition conditioned on the resolved velocity field $\tilde{\boldsymbol{u}}$, where $\boldsymbol{\psi}$ denotes the composition sample space of $\boldsymbol{\phi}$. Then the LES mean composition is $\tilde{\boldsymbol{\phi}} = \int \boldsymbol{\psi} f d\boldsymbol{\psi}$ and the LES mean density is $\bar{\rho} = 1/\int f/\rho(\boldsymbol{\psi}) d\boldsymbol{\psi}$. In the traditional filtering viewpoint in LES/PDF [6,28], the overline "−" denotes the filtering operation. Practically, both viewpoints of LES/PDF do not lead to substantially different partial differential equations to be solved.

The exact transport equation of $f(\boldsymbol{\psi};\boldsymbol{x},t)$

$$\frac{\partial f}{\partial t} + \nabla\cdot[f(\tilde{\boldsymbol{u}} + \widetilde{\boldsymbol{u}|\boldsymbol{\psi}})] = -\frac{\partial}{\partial \psi_\alpha}\left[f\left(\frac{1}{\bar{\rho}}\overline{\nabla\cdot(\rho\Gamma_{(\alpha)}\nabla\phi_\alpha)|\boldsymbol{\psi}} + S_\alpha(\boldsymbol{\psi})\right)\right], \quad (1)$$

is derived in [27–29], where the summation convention applies over the subscript "α", except to suffice in brackets, and S_α is the chemical reaction source term. In the right-hand-side (RHS) of Eq. (1), the conditional diffusion term

$$\gamma_\alpha(\boldsymbol{\psi},\boldsymbol{x},t) \equiv \frac{1}{\bar{\rho}}\overline{\nabla\cdot(\rho\Gamma_{(\alpha)}\nabla\phi_\alpha)|\boldsymbol{\psi}} \quad (2)$$

is modeled by

$$\gamma_\alpha(\boldsymbol{\psi},\boldsymbol{x},t) = -\Omega_m(\psi_\alpha - \tilde{\phi}_\alpha) + \widetilde{\mathcal{D}} \quad (3)$$

in LES/PDF, where the first term in the RHS is the interaction-by-exchange with the mean (IEM) mixing model [30,31] and $\mathcal{D} \equiv \frac{1}{\bar{\rho}}\nabla\cdot(\bar{\rho}\Gamma\nabla\phi)$ is the mean drift term in the PDF method. This IEM model with molecular transport and the corresponding numerical method are developed in [32,33]. This implementation does not give rise to the spurious production of scalar variance and includes the effects of differential diffusion. However, in this study we only use a single mixture diffusivity Γ, assuming unity Lewis numbers.

Eq. (1) with the model Eq. (3) is solved by a particle method

$$d\boldsymbol{X}^*(t) = \left(\tilde{\boldsymbol{u}} + \frac{\nabla\bar{\rho}\Gamma_T}{\bar{\rho}}\right)^* dt + \sqrt{2\Gamma_T^*}d\boldsymbol{W}, \quad (4)$$

$$d\boldsymbol{\phi}^*(t) = -\Omega_m^*(\boldsymbol{\phi}^* - \tilde{\boldsymbol{\phi}}^*)dt + \widetilde{\mathcal{D}}^* dt + \boldsymbol{S}(\boldsymbol{\phi}^*)dt. \quad (5)$$

using the highly-scalable HPDF code [13] with second-order accuracy in space and time, where $\boldsymbol{X}^*(t)$ is the particle position, $\boldsymbol{W}$ is an isotropic, vector-valued Wiener process, $\tilde{\boldsymbol{\phi}}$ is the resolved scalars in LES. The superscript "*" on mean quantities denotes evaluating the quantity at $\boldsymbol{X}^*(t)$ by interpolation. The scalar mixing frequency is modeled as

$$\Omega_m = C_\phi(\Gamma + \Gamma_T)/\Delta^2, \quad (6)$$

with a model constant $C_\phi = 5$ for all the species in this study. Here, the value of C_ϕ is determined by

Table 1
Parameters of study for DNS and LES/PDF.

Run	Re	H (mm)	N_x	N_y	N_z	Δx (μm)
DNS	2510	0.72	576	672	384	15.0
	9017	1.37	864	1008	576	19.0
LES/PDF	2510	0.72	72	84	48	120.0
	9017	1.37	108	126	72	152.2

the sensitivity study on the statistics discussed in Section 3. In Eq. (5), the realizability and the normalization condition of $\boldsymbol{\phi}^*$ is achieved by imposing a lower limit on the mixing frequency. It is noted that this adjustment is small so that it does not degrade the second-order accuracy of the numerical scheme [32]. The molecular transport properties used in LES are approximated by an empirical fit to the DNS data as $\mu/\bar{\rho} = v_0(\widetilde{T}/T_0)^{1.67}$ and $\Gamma = c_0 v_0(\widetilde{T}/T_0)^{1.77}$, where $v_0 = 3.83 \times 10^{-5}\mathrm{m}^2/\mathrm{s}$, $c_0 = 1.416$, and $\widetilde{T}$ is obtained from the PDF calculations. In the present PDF calculations, typically $N_{pc} = 20$ particles are used in each cell. For the computation of combustion chemistry with the same CO/H_2 mechanism used in DNS, the ISAT algorithm is applied to obtain the time integration of the reaction rate $\boldsymbol{S}(\boldsymbol{\phi})$ in Eq. (5) [8,9].

The coupling algorithm of the density from the Monte Carlo PDF code to the finite volume LES code is important and challenging [12,34]. In this study, we used the LES solver with the third-order bounded QUICK scheme [25] to evolve an additional scalar equation

$$\bar{\rho}\frac{\partial \tilde{v}}{\partial t} + \bar{\rho}\tilde{\boldsymbol{u}}\cdot\nabla\tilde{v} = \nabla\cdot(\bar{\rho}(\Gamma+\Gamma_T)\nabla\tilde{v}) + S_v \qquad (7)$$

for the resolved specific volume $\tilde{v}$, which is the inverse of the density $\bar{\rho}$. Here, S_v is the logarithmic rate of volume expansion primarily due to heat release, and it is evaluated by

$$S_v = \frac{2\langle m^*(v^*(t+\Delta t) - v^*(t))\rangle_c}{\Delta t\langle m^*(v^*(t+\Delta t) + v^*(t))\rangle_c}, \qquad (8)$$

where m^* is the mass of an individual particle, $v^*(t)$ the particle's specific volume as a function of time, Δt the time step, and the operator $\langle\cdot\rangle_c$ denotes taking the average over a LES grid cell with the cloud-in-cell approach. The consistency of the two-way coupling algorithm has been verified in several flame testing cases with the steady flamelet model [34].

3. Comparisons of DNS and LES/PDF

The LES/PDF of the non-premixed CO/H_2 temporally evolving jet flame is performed up to $t = 40t_j$ for both low- and high-Re cases (see Table 1). The total number of grid points in LES/PDF is 1/512 of that in DNS. The computational time for a high-Re LES/PDF run with 19.6 million particles is about 500 CPU hours on the Cray XT5 Jaguar supercomputer.

The instantaneous contours of mixture fraction ξ in an x–y plane are shown in Fig. 2 from DNS (upper half plane) and LES/PDF (lower half plane). Here, ξ is based on Bilger's formulation [35], which is a conserved scalar and shows the mixing characteristics. From the DNS results, we can see that at $20t_j$ the turbulent jet is in the transition stage with very strong straining in two shear layers between the central jet and co-flows, and subsequently the turbulent jet becomes fully developed at $40t_j$. The contours from the LES/PDF basically capture the large-scale structures of this jet flame, but most of the small-scale, sheet-like structures are below the resolved scales.

For quantitative studies, we first compare the temporal evolution of mixture fraction at $t = 10,20,30,40t_j$ for $Re = 9079$ in DNS and LES/PDF. The first row of Fig. 3 shows the resolved mean mixture fraction $\langle\tilde{\xi}\rangle_{xz}$, the resolved root mean square (rms) $\langle\xi''\rangle_{xz} = (\langle(\tilde{\xi})^2\rangle_{xz} - \langle\tilde{\xi}\rangle^2_{xz})^{1/2}$, and the total rms $\langle\xi''\rangle^{\mathrm{total}}_{xz} = \left(\langle\widetilde{\xi^2}\rangle_{xz} - \langle\tilde{\xi}\rangle^2_{xz}\right)^{1/2}$, where $\langle\cdot\rangle_{xz}$ denotes the average over an x–z plane. The agreement is very good except the spreading of the jet appears to be slightly faster at the latest time $40t_j$ in the LES/PDF. The resolved mean and rms temperature and mass fractions of the major species Y_{CO} and Y_{CO_2} are also shown in Fig. 3. Overall good agreement of the LES/PDF results with the DNS is observed. The discrepancy between LES/PDF and DNS at $t = 40t_j$ may be related to the faster spreading rate of the jet in

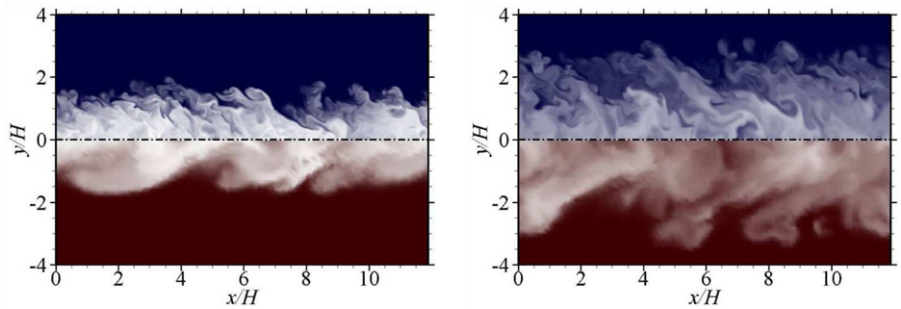

(a) $t = 20t_j$ (b) $t = 40t_j$

Fig. 2. Contours of mixture fraction $0 \leqslant \xi \leqslant 1$ color coded from light to dark on an x–y plane cut from DNS (upper half) and LES/PDF (lower half) for $Re = 9079$. (For interpretation of the references to color in this figure legend, the reader is referred to the web version of this article.)

LES/PDF as shown in the evolution of mixture fraction. It is noted that, compared to the high-*Re* case, the LES/PDF results for $Re = 2510$ are found to be in a much better agreement with DNS for the statistics shown in Fig. 3, and here the mean and rms profiles of the low-*Re* LES/PDF are not shown. As may be observed, the total rms is only slightly larger than the resolved rms, indicating that the LES grid is sufficient fine to resolve the energy-containing scales. The greatest observed difference in the resolved and total rms is for Y_{CO_2} at $t = 10t_j$.

Furthermore, the mean profiles of the dissipation rate of mixture fraction are compared in the last row in Fig. 3. Here, the scalar dissipation rate is $\chi = 2\Gamma\nabla\xi \cdot \nabla\xi$ in DNS, and is modeled as $\tilde{\chi} = 2(\Gamma\nabla\tilde{\xi} \cdot \nabla\tilde{\xi} + \Omega_m \xi''^2)$ in LES/PDF where $\xi''^2 = \tilde{\xi^2} - (\tilde{\xi})^2$ is the residual variance of mixture fraction and Ω_m is defined by Eq. (6). We observe that $\langle\tilde{\chi}\rangle_{xz}$ is underestimated at the early stage, because the small-scale straining motions with very high χ are filtered in LES/PDF (also refer to Fig. 2(a)). It appears that, at $t = 20t_j$ in LES/PDF, the very high local dissipation rates are not critical for the prediction of the mean mixture fraction, because the scalar dispersion is mainly controlled by large-scale motions at the early stage.

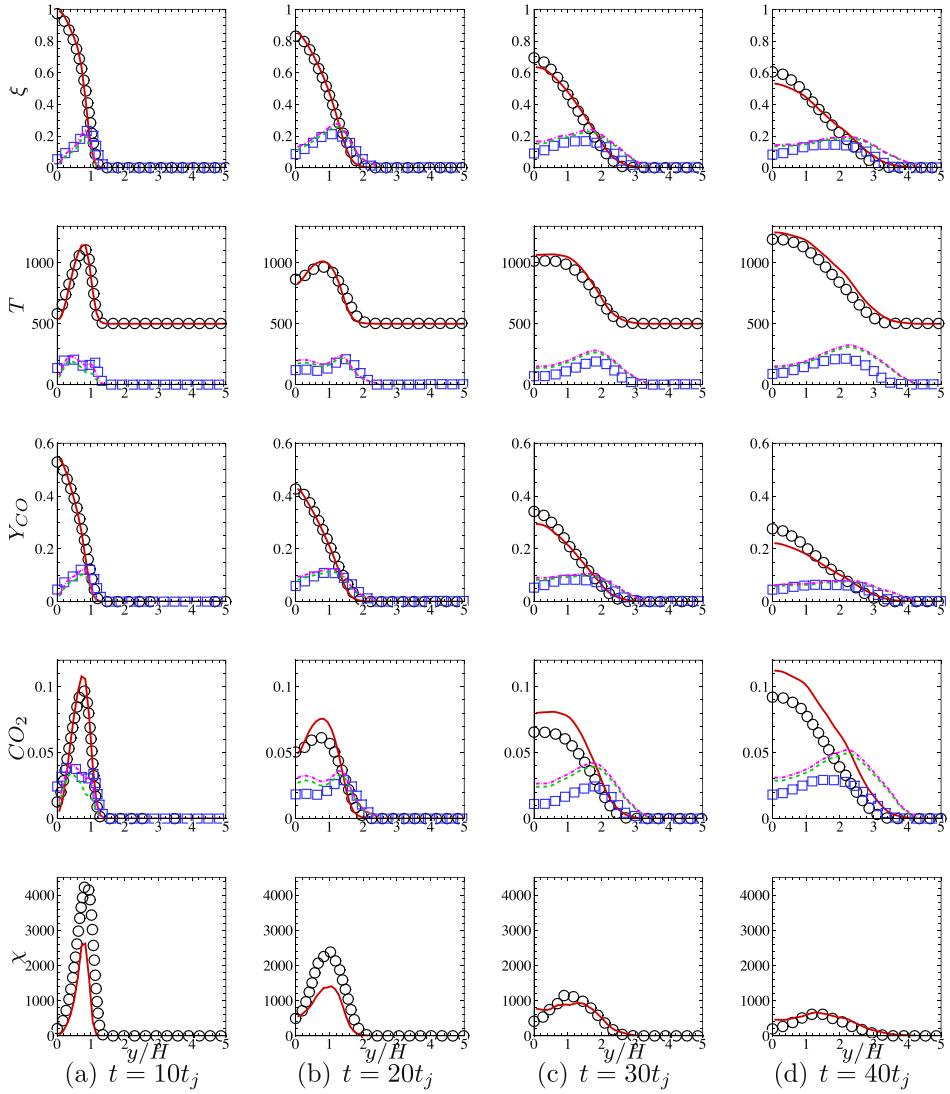

Fig. 3. Mean and rms profiles of ξ, T, Y_{CO} and Y_{CO_2}, and mean profiles of χ at $t = 10,20,30,40t_j$ from DNS and LES/PDF for $Re = 9079$ (○: mean in DNS; solid line: mean in LES/PDF; □: rms in DNS; dashed line: resolved rms in LES/PDF; dash-dotted line: total rms in LES/PDF).

Since mixing is initially rapid enough relative to reaction at the low *Da* in this flame, strong turbulence–chemistry interactions can result in local extinction. The DNS results show that the maximum local extinction occurs near $t = 20t_j$. The comparisons of DNS and LES/PDF for the mean temperature in the whole domain conditioned on mixture fraction at $t = 0{,}20{,}40t_j$ for both low and high-*Re* cases are shown in Fig. 4. At $t = 20t_j$, the high-*Re* case has a higher degree of extinction than that in the low-*Re* case [22]. Both cases re-ignite following extinction, and at $t = 40t_j$ the high-*Re* case is not as fully re-ignited as the low-*Re* case. We can see that the low-*Re* results are in a very good agreement with DNS. The high-*Re* results show slight overprediction of the conditional mean temperature, which is consistent with that shown in the mean temperature profiles in Fig. 3.

4. Multi-scalar mixing

Since combustion requires that fuel and oxidizer be mixed at the molecular level, the modeling of the mixing of compositions is crucial in LES/PDF modeling approach. Benefiting from the available DNS database [22], the term of mixing Eq. (2) in the PDF transport equation can be exactly extracted from DNS. This can be considered as a diffusion velocity of multiple compositions in composition space, and defines the "streamlines" in the composition space $\boldsymbol{\psi}$ [19].

In LES/PDF, for the general particle we can define $\gamma_\alpha^* \equiv -\Omega_m^*\left(\phi_\alpha^* - \tilde{\phi}_\alpha^*\right) + \widetilde{\mathcal{D}}^*$ to be the modeled particle velocity in composition space implied by Eq. (3). By taking the conditional average of Eq. (4) in an x–z plane, we obtain

$$\begin{aligned}\langle \gamma_\alpha | \phi = \boldsymbol{\psi} \rangle_{xz} &\equiv \langle\langle \gamma_\alpha^* | \phi^* = \boldsymbol{\psi} \rangle\rangle_{xz} \\ &= -\langle\langle \Omega_m^* | \boldsymbol{\psi} \rangle\rangle_{xz} (\psi_\alpha - \hat{\phi}_\alpha(\boldsymbol{\psi})) \\ &\quad + \langle\langle \widetilde{\mathcal{D}}^* | \boldsymbol{\psi} \rangle\rangle_{xz}, \end{aligned} \tag{9}$$

where $\langle\cdot\rangle$ denotes the local conditional average at $\boldsymbol{X}$, and

$$\hat{\phi}_\alpha(\boldsymbol{\psi}) \equiv \langle\langle \Omega_m^* \tilde{\phi}_\alpha^* | \boldsymbol{\psi} \rangle\rangle_{xz} / \langle\langle \Omega_m^* | \boldsymbol{\psi} \rangle\rangle_{xz}. \tag{10}$$

We find that in general the mean drift term is relatively small in the RHS of Eq. (9) in this flame, so the streamlines tend to be attracted to a manifold

$$\mathcal{M}(\boldsymbol{\psi}) \equiv \|\boldsymbol{\psi} - \hat{\boldsymbol{\phi}}(\boldsymbol{\psi})\|_2 = 0. \tag{11}$$

In the RANS/PDF context, Eq. (10) reduces to a single point $\hat{\phi}_\alpha = \langle \phi_\alpha^* \rangle_{xz}$ and all the streamlines are straight lines through $\langle \phi_\alpha^* \rangle_{xz}$, while in the LES/PDF context, the attracting manifold could be Eq. (11) with

$$\hat{\phi}_\alpha \approx \langle\langle \tilde{\phi}_\alpha^* | \boldsymbol{\psi} \rangle\rangle_{xz}. \tag{12}$$

Here, we assume the weak dependence between Ω_m^* and $\tilde{\boldsymbol{\phi}}^*$, which will be justified subsequently.

The PDFs of mixture fraction $f(\psi_\xi)$ and the normalized conditional diffusions $t_j \langle \gamma_\xi | \psi_\xi \rangle_{xz}$ on the x–z plane-cut at $y/H = 0$ for the high-*Re* DNS and LES/PDF are shown in Fig. 5. The statistics are obtained from a slab of $N_x \times N_z \times 8$ grid points in DNS and about $N_x \times N_z \times N_{pc}$ particles in LES/PDF. The LES/PDF results qualitatively agree with the DNS results but have some quantitative differences, which implies some discrepancies of the high-order moments of ξ. From Eqs. (3) and (6), the underprediction of $t_j \langle \gamma_\xi | \psi_\xi \rangle_{xz}$ suggests that the model of Ω_m may not be very accurate, at least in some local regions. This causes the slower relaxation of the $f(\psi_\xi)$ in Eq. (1), resulting in the slight underprediction of the mean mixture fraction in Fig. 3.

In the present study of multi-scalar mixing, we chose two representative scalar fields: the mixture fraction and the mass fraction of the major product Y_{CO_2} as a progress variable, and define two corresponding diffusion velocities $\gamma_1 = \langle \gamma_\xi | \psi_\xi, \psi_{CO_2} \rangle_{xz}$ and $\gamma_2 = \langle \gamma_{CO_2} | \psi_\xi, \psi_{CO_2} \rangle_{xz}$, and the velocity

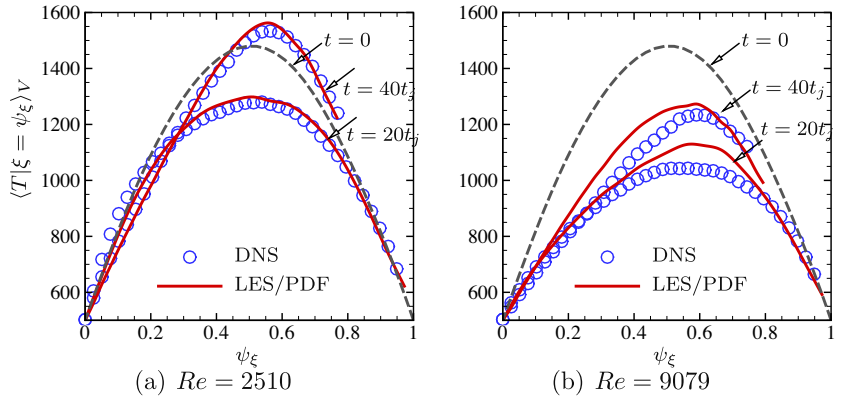

Fig. 4. The mean temperature in the whole domain conditioned on mixture fraction at $t = 0{,}20{,}40t_j$ in low and high Reynolds numbers cases.

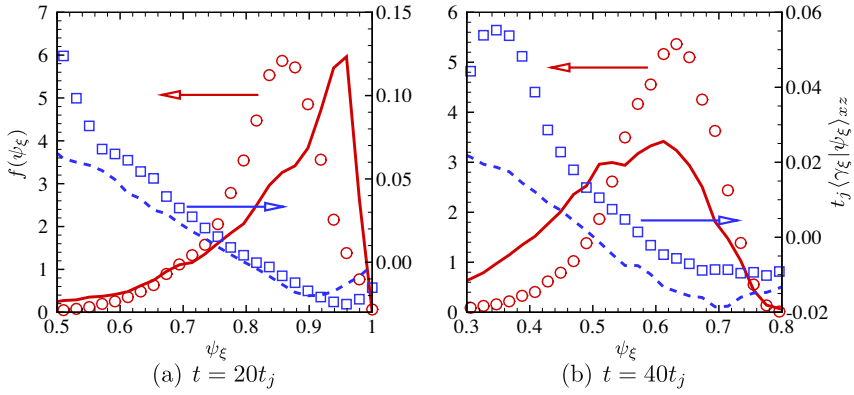

Fig. 5. Normalized conditional diffusion and PDFs of mixture fraction at $y/H = 0$ in DNS (symbols) and LES/PDF (lines) for $Re = 9079$.

magnitude $\gamma = \sqrt{\gamma_1^2 + \gamma_2^2}$. The joint PDFs $f(\psi_\xi, \psi_{CO_2})$ and the normalized conditional means of the diffusion velocity magnitude γt_j from DNS and LES/PDF at $y/H = 0$ are shown in Fig. 6. At $t = 20t_j$ when the jet is during the transition stage we can see an attracting manifold in the composition space, while at $t = 40t_j$ when the jet becomes fully turbulent the joint PDF tends to

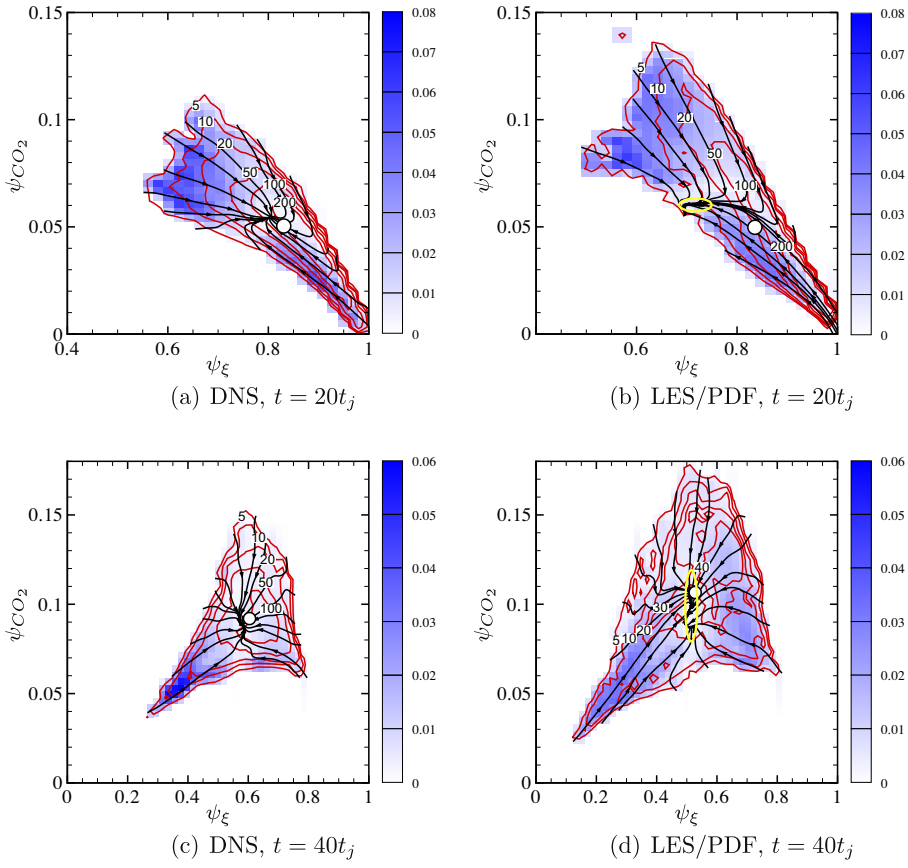

Fig. 6. Contours of joint PDFs $f(\psi_\xi,\ \psi_{CO_2})$ (red lines with labeled contour values) and the normalized conditional mean diffusion velocity magnitude γt_j (blue shading) from DNS and LES/PDF at $t = 20{,}40t_j$ and $y/H = 0$. The mean scalars $(\langle\xi\rangle_{xz},\ \langle Y_{CO_2}\rangle_{xz})$ are indicated by a circle. The region of $\mathcal{M}(\psi_\xi, \psi_{CO_2}) \approx 0$ is marked by yellow open ovals. (For interpretation of the references to color in this figure legend, the reader is referred to the web version of this article.)

be closer to the joint normal distribution and the streamlines are relatively close to the radii centered at $(\langle\xi\rangle_{xz}, \langle Y_{CO_2}\rangle_{xz})$ implied by the IEM model in LES/PDF.

The formation of the manifold in composition space may be related to the large-scale coherent scalar structures, which exists near the transition regions from laminar flow to turbulent flow. We observe the manifold exhibits complex, non-linear behavior, which is similar to that shown in Fig. 5(a), near the interfaces of shear layers, e.g., at $y/H = 1$ and $t = 20t_j$, and at $y/H = 2$ and $t = 40t_j$ (not shown). This implies that it would be a challenge for the IEM model applied in the RANS/PDF, because in this case all the streamlines are radii pointing to the plane-averaged values. On the other hand, the LES/PDF results in Fig. 6 show some qualitative agreement on the joint PDF and the location of the manifold with DNS. According to Eqs. (11) and (12), the streamlines in LES/PDF appear to be attracted to a manifold $\mathcal{M}(\psi_\xi, \psi_{CO_2}) \approx 0$. More quantitative analysis on the formation of the manifold in composition space and its implications in LES/PDF will be considered in future work.

5. Conclusions

A detailed comparative study of DNS and LES/PDF of a non-premixed CO/H_2 temporally evolving planar jet flame with skeletal chemistry is reported. The LES/PDF methodology is implemented using the highly scalable NGA/HPDF codes with second-order accuracy in space and time. The recently developed IEM mixing model with molecular transport and the two-way coupling algorithm based on the specific volume have been employed. The computational cost in the current LES/PDF is less than 1/1000 of the corresponding DNS.

The performance of the hybrid LES/PDF methodology is assessed through detailed *a posteriori* comparisons with DNS of the same flame. The comparison shows overall good agreement of the temporal evolution of the temperature and mass fractions of major chemical species, as well as the prediction of local extinction and reignition. With the filter size $\Delta = 8\Delta x$ of DNS, better predictions are obtained in the low-*Re* LES/PDF than in the high-*Re* case. Based on the accuracy of the current LES/PDF calculations, it is reasonable to suppose that the similar accuracy would be achieved at higher *Re* with the same grid spacing relative to that required for DNS (i.e., high-fidelity LES). If however an LES grid spacing that is comparable to the turbulent integral scale were used, then it is an open question how accurate the current LES/PDF modeling would be. The capability of LES/PDF for reactive flow in industrial applications at higher Re cannot be validated in detail until the completion of relevant DNS with a larger dynamic range of computational scales.

The critical issue in the PDF method, the modeling of multi-scalar mixing in turbulent reacting flows, is investigated by the comparisons of the conditional diffusion term in the PDF transport equation, which can be exactly extracted from DNS and LES/PDF results. The formation and the location of an attracting manifold from the streamlines of the diffusion velocity in composition space is analyzed. The DNS exhibits the manifold based on the plane-averaging statistics at the early stage, when the transition from laminar flow to turbulent flow shows large-scale coherent structures with small-scale fluctuations. The LES/PDF results show qualitative agreement for the manifold and joint PDFs of scalars.

The success of the current implementation of LES/PDF with the IEM mixing model is expected to stimulate more challenging cases using LES/PDF in the future, including partially premixed and premixed turbulent jet flames. The current DNS and LES/PDF data also provide an excellent testbed for detailed study on the modeling of multi-scalar mixing in RANS/PDF, LES/PDF, and self-conditioned LES/PDF [27] with different mixing models.

Acknowledgments

The authors are grateful to O. Desjardins for the help of the NGA code, E.R. Hawkes and H. Kolla for the support on the post-processing of the DNS data, and P.P. Popov for the help of the two-way coupling algorithm. This research is supported by the Combustion Energy Frontier Research Center, an Energy Frontier Research Center funded by the US Department of Energy (DOE), Office of Science, Office of Basic Energy Sciences under Award No. DE-SC0001198. Computer allocations were awarded by DOE's Innovative and Novel Computational Impact on Theory and Experiments (INCITE) Program. This research used resources of the National Center for Computational Sciences at Oak Ridge National Laboratory (NCCS/ORNL) which is supported by the Office of Science of the US DOE under Contract No. DE-AC05-00OR22725.

References

[1] J.H. Chen, *Proc. Combust. Inst.* 33 (2011) 99–123.
[2] L. Selle, G. Lartigue, T. Poinsot, et al., *Combust. Flame* 137 (2004) 489–505.
[3] S. Menon, N. Patel, *AIAA J.* 44 (2006) 709–723.
[4] M. Boileau, G. Staffelbach, B. Cuenot, T. Poinsot, C. Berat, *Combust. Flame* 154 (2008) 2–22.
[5] S.B. Pope, *Prog. Energy Combust. Sci.* 11 (1985) 119–192.

[6] P.J. Colucci, F.A. Jaberi, P. Givi, S.B. Pope, *Phys. Fluids* 10 (1998) 499–515.
[7] D.C. Haworth, *Prog. Energy Combust. Sci.* 36 (2010) 168–259.
[8] S.B. Pope, *Combust. Theory Model.* 1 (1997) 41–63.
[9] L. Lu, S.R. Lantz, Z. Ren, S.B. Pope, *J. Comput. Phys.* 228 (2009) 5490–5525.
[10] H. Pitsch, *Annu. Rev. Fluid Mech.* 38 (2006) 453–482.
[11] M.R.H. Sheikhi, T.G. Drozda, P. Givi, F.A. Jaberi, S.B. Pope, *Proc. Combust. Inst.* 30 (2005) 549–556.
[12] V. Raman, H. Pitsch, *Proc. Combust. Inst.* 31 (2007) 1711–1719.
[13] H. Wang, S.B. Pope, *Proc. Combust. Inst.* 33 (2011) 1319–1330.
[14] V. Eswaran, S.B. Pope, *Phys. Fluids* 31 (1988) 506–520.
[15] D.H. Wang, C.N. Tong, *Phys. Fluids* 14 (2002) 2170–2185.
[16] Z.Y. Ren, S.B. Pope, *Combust. Flame* 136 (2004) 208–216.
[17] S. Mitarai, J.J. Riley, G. Kosaly, *Phys. Fluids* 17 (2005) 047101.
[18] J. Cai, M.J. Dinger, W. Li, C.D. Carter, M.D. Ryan, C. Tong, *J. Fluid Mech.* 685 (2011) 495–531.
[19] A. Juneja, S.B. Pope, *Phys. Fluids* 8 (1996) 2161–2184.
[20] B.L. Sawford, S.M. de Bruyn Kops, *Phys. Fluids* 20 (2008) 095106.
[21] D.W. Meyer, R. Deb, *Phys. Fluids* 24 (2012) 025103.
[22] E.R. Hawkes, R. Sankaran, J.C. Sutherland, J.H. Chen, *Proc. Combust. Inst.* 31 (2007) 1633–1640.
[23] E.R. Hawkes, R. Sankaran, J.H. Chen, S.A. Kaiser, J.H. Frank, *Proc. Combust. Inst.* 32 (2009) 1455–1463.
[24] N. Punati, J.C. Sutherland, A.R. Kerstein, E.R. Hawkes, J.H. Chen, *Proc. Combust. Inst.* 33 (2011) 1515–1522.
[25] O. Desjardins, G. Blanquart, G. Balarac, H. Pitsch, *J. Comput. Phys.* 227 (2008) 7125–7159.
[26] C.D. Pierce, P. Moin, *J. Fluid Mech.* 504 (2004) 73–97.
[27] S.B. Pope, *J. Fluid Mech.* 652 (2010) 139–169.
[28] F.A. Jaberi, P.J. Colucci, S. James, P. Givi, S.B. Pope, *J. Fluid Mech.* 401 (1999) 85–121.
[29] F. Gao, E.E. O'Brien, *Phys. Fluids A* 5 (1993) 1282–1284.
[30] J. Villermaux, J.-C. Devillon*Proc. of the 2nd Int. Symp. on Chem. React. Eng.*, vol. 26, Elsevier, New York, USA, 1972, pp. 1–13.
[31] C. Dopazo, E. O'Brien, *Acta Astronaut.* 1 (1974) 1239–1266.
[32] R. McDermott, S.B. Pope, *J. Comput. Phys.* 226 (2007) 947–993.
[33] S. Viswanathan, H. Wang, S.B. Pope, *J. Comput. Phys.* 230 (2011) 6916–6957.
[34] P.P. Popov, S. Viswanathan, H. Wang, S.B. Pope, in: *7th US National Technical Meeting of the Combustion Institute*, March, 2011, Atlanta, Georgia, USA, pp. 1C16.
[35] R.W. Bilger, S.H. Stårner, R.J. Kee, *Combust. Flame* 80 (1990) 135–149.